Scientia Iranica, Vol. 8, No. 2, pp 110-122
© Sharif University of Technology, April 2001

SCIENTIA
IRANICA

A Field Boundary Element Method for Large Deformation Analysis of Hyperelastic Problems

G. Karami* and D. Derakhshan[1]

In this paper, a Field Boundary Element Method (FBEM) is applied to hyperelastic Mooney-Rivilin type materials to exhibit the finite strain large deformation in two and three dimensional problems. The field BEM formulation is developed using the weak forms of integrals employing the equilibrium equations and the proper fundamental displacement solution. The divergence theorem is then employed to separate the boundary and the field integrals. The boundary integrals represent the standard linear elastic (small strain) behavior, whereas the field integrals come from nonlinear terms due to nonlinear geometrical and material behaviors. The geometrical nonlinearities appear in two parts; resulting from the nonlinearities in kinematical relations and the second part comes from the nonlinear moving tractions on the boundary. Due to the mere dependency of constitutive relations on deformation or strain tensor, a partial differentiation of displacement integral equations with respect to source point is needed to obtain the gradient of displacement directly.

The computational framework is total-Lagrangian presentation, in which the stiffness matrices are constructed at the initial configuration (reference coordinate) only. The discretized formulation is based on the linear boundary elements and bilinear field elements. The Newton-Raphson and Broyden rank-1 schemes are applied to the system of nonlinear equations because of the confidence on quadratic rate of convergency. An incremental loading procedure will be implemented to insure the convergency and accuracy. The accuracy of the results are discussed through solving several examples.

INTRODUCTION

Large deformation analysis is becoming a necessity nowadays, in constructing a real deformation analysis for an optimum design of mechanical and structural elements. Also, considering the usage of modern rubber-made materials in practice, hyperelastic material behavior assumption proves to be more practical. The implementation of nonlinear material modelings in the numerical algorithms, such as boundary elements, is a step forward in analysis and design.

Nonlinearities in solid mechanics are categorized into two classes of geometrical and material nonlinearities. The source of geometric nonlinearities is the nonlinear terms in the kinematical relations. The source of material nonlinearities, on the other hand, is the nonlinear terms in the constitutive equations which, in turn, is categorized into several forms of hyperelasticity, plasticity, viscoelasticity and other forms. The nonlinear kinematical and material relations have substantial impact on the final deformation and equilibrium conditions whenever sever loading is encountered. The material and geometrical nonlinear terms can also produce coupled terms which play essential roles in consistency and bifurcation of nonlinear equations [1].

The nonlinear rubber-like Mooney-Rivilin type constitutive relations associated with incompressibility condition, in general, are employed in the work presented here. This model could be applied to most synthetic substances like isotropic polymers and matrix of composites [2-5]. The material nonlinearity constitutive relations for such materials are written in various forms; some in terms of deformation or strain tensors, some in terms of product of displacement and their gradients and some in terms of nonlinear combination of displacement and strain tensors [6-8].

In this paper, the continuum-based hyperelastic constitutive relations based on the fundamentals of

*. *Corresponding Author, Department of Mechanical Engineering, School of Engineering, Shiraz University, Shiraz, I.R. Iran.*

1. *Department of Mechanical Engineering, School of Engineering, Shiraz University, Shiraz, I.R. Iran.*

thermodynamics are employed [9,10]. The boundary integral equations are constituted of the displacement gradients. The order of singularities of the integrands are increased, so that the hyper and strongly singular integrals would be created. The evaluation of such integrals is accomplished with a great deal of difficulty. However, strong mathematical-based regularization schemes [11-13] are used to evaluate such integrals. Evaluation of the discretized form of the field integrals consumes a lot of time at each load increment. Total-Lagrangian approach reduces this time considerably due to its independency of the current configuration. To solve the resulted system of extremely nonlinear equations, a powerful method based on Newton-Raphson method is employed in company with Broyden rank-1 update scheme [14]. The method converged with a satisfactory rate even in very large deformation problems.

THE GOVERNING EQUATIONS

Kinematical Relations

The general form of kinematical relations may be written in the following form [8]:

$$\mathbf{C} = \mathbf{G} + \mathbf{H} + \mathbf{H}^T + \mathbf{H}^T.\mathbf{H}, \tag{1}$$

where $\mathbf{C}$, $\mathbf{H}$ and $\mathbf{G}$ represent the deformation tensor, displacement and metric tensors, respectively, in material coordinates. The relation between the deformation tensor and the Green strain tensor, $\mathbf{E}$, is defined according to:

$$\mathbf{E} = \frac{1}{2}(\mathbf{C} - \mathbf{G}) = \frac{1}{2}(\mathbf{H} + \mathbf{H}^T + \mathbf{H}^T.\mathbf{H}). \tag{2}$$

In the right side of Equation 1, the quadratic term, which is the product of the displacement gradients, is the source of the geometrical nonlinearity in kinematical relations. The spatial form of kinematical relations may be written as:

$$\mathbf{e} = \frac{1}{2}(\mathbf{g} - \mathbf{b}^{-1}), \tag{3}$$

where $\mathbf{b}^{-1}$ is the total finger deformation tensor, the counterpart of the deformation tensor in spatial coordinate. $\mathbf{g}$ is the spatial metric tensor and $\mathbf{e}$ is the Cauchy strain tensor. Note that $\mathbf{b} = \mathbf{F}.\mathbf{G}.\mathbf{F}^T$, where $\mathbf{F} = \mathbf{Sh}.(\mathbf{G} + \mathbf{H})$ denotes the deformation gradient and $\mathbf{Sh}$ represents shifter operator which is a metric tensor between the two coordinate systems, i.e., it can evaluate the components of a tensor from material coordinates to spatial coordinates and vice-versa.

Stresses and Tractions

Depending on the coordinate view point of either deformed or undeformed state, definition of the stress tensor may be represented in one of the following four different forms. If load and the differential subjected area are defined in material coordinates, the stress is called second Piola-Kirchhoff stress tensor, denoted by $\mathbf{\Sigma}$. If load is measured in material coordinates but the area is measured in deformed coordinates the resultant is called first Piola-Kirchhoff stress tensor, $\mathbf{S}$. Through defining both the load and the area in spatial coordinates, Cauchy or true stress $\boldsymbol{\sigma}$ would be the outcome. The other definition is related to Kirchhoff stress tensor $\boldsymbol{\tau}$ which is obviously expressed by the undeformed area and the spatial measuring load. These stress definitions may be transformed to each other by pre and post multiplying of $\mathbf{F}$, the deformation gradient tensor. For example, Cauchy stress relates to second Piola-Kirchhoff stress by the following relation:

$$\boldsymbol{\sigma} = \frac{1}{J}\mathbf{F}.\mathbf{\Sigma}.\mathbf{F}^T, \tag{4}$$

where $J = \det[\mathbf{F}]$ stands for the dilatations or Jacobian of transformation. Kirchhoff and Cauchy stresses have a simpler relation as follows:

$$\boldsymbol{\tau} = J\boldsymbol{\sigma} \ . \tag{5}$$

Similar to the strain tensor decomposition, the stress tensor may be decomposed into a linear and a nonlinear part, having the following form:

$$\mathbf{\Sigma} = \mathcal{A}\colon \mathbf{H} + \overset{n}{\mathbf{\Sigma}}, \tag{6}$$

where $\mathcal{A}$ and $\overset{n}{\mathbf{\Sigma}}$ represent linear elasticity tensor and whole nonlinear stress terms (containing geometrical, material and their coupled), respectively. The linear elastic tensor is addressed in continuum mechanics text books (e.g., [7 or 8]). The material representation of such tensor can be written as follows:

$$\mathcal{A}^{IJKL} = \frac{2\mu\nu}{1-2\nu}G^{IJ}G^{KL} - \mu(G^{IK}G^{JL} + G^{IL}G^{JK}),$$

where μ and ν are the shear modulus and Poisson's ratio, respectively.

Tractions are distributed loads over the boundary of the body. There are also different definitions for the traction vector. The Cauchy traction is defined as:

$$\mathbf{t} = \boldsymbol{\sigma}.\mathbf{n}, \tag{7}$$

where $\mathbf{n}$ denotes the normal unit vector of the deformed area and is measured in spatial coordinates. Similar definition as in Equation 7 relates the material or undeformed traction $\mathbf{T}$ to the stress $\mathbf{\Sigma}$ and the normal material vector $\mathbf{N}$ to the area as:

$$\mathbf{T} = (\mathbf{H} + \mathbf{G}).\mathbf{\Sigma}.\mathbf{N} = \frac{\mathrm{ds}}{\mathrm{dS}}\mathbf{Sh}^T.\mathbf{t}, \tag{8}$$

where ds and dS are the deformed and undeformed areas, respectively.

Constitutive Relations

As a result of the first and second law of thermodynamics, the hyperelastic constitutive equations are derived using simple partial differentiation with respect to the deformation or strain tensors [9,10,15]. Incompressible Mooney-Rivilin rubber-like materials are good examples for hyperelastic materials. Denoting the free energy density by Ψ and assuming ρ_0 as the density of media in material coordinates, this property for a group of hyperelastic materials is defined by [3]:

$$\Psi(\mathbf{C}) = \frac{1}{4\rho_0}\mu[(\frac{1}{2}+\theta)(I_1-3)+(\frac{1}{2}-\theta)(I_2-3)]. \tag{9}$$

I_1, I_2 and I_3 are the deformation tensor invariants, i.e.,

$$I_1 = tr_G[\mathbf{C}] = \mathbf{C}:\mathbf{G}, \qquad I_2 = tr_G[\mathbf{C}^{-1}] = \mathbf{C}^{-1}:\mathbf{G},$$

$$I_3 = \det \mathbf{C}$$

with the following properties:

$$\frac{\partial I_1}{\partial \mathbf{C}} = \mathbf{G}, \qquad \frac{\partial I_2}{\partial \mathbf{C}} = -\mathbf{C}^{-2} \qquad \frac{\partial I_3}{\partial \mathbf{C}} = \det(\mathbf{C})\mathbf{C}^T,$$

where tr_G and det stand for the trace and determinant operators (in material coordinates), respectively. The incompressibility condition would require that:

$$I_3 = \det \mathbf{C} = 1.$$

Also, Equation 9 is defined under the following conditions:

$$\mu > 0, \qquad -\frac{1}{2} \le \theta \le \frac{1}{2},$$

where θ appears, here, as an independent material property. According to hyperelastic relations based on the first and second laws of thermodynamics, second Piola-Kirchhoff stress is obtained immediately [7,8]:

$$\mathbf{\Sigma} = 2\rho_0\frac{\partial \Psi}{\partial \mathbf{C}} = \mu(\frac{1}{2}+\theta)\mathbf{G} - \mu(\frac{1}{2}-\theta)\mathbf{C}^{-2} - \Pi_{hyd}\mathbf{C}^{-1}, \tag{10}$$

where Π_{hyd} is an augmented variable due to hydrostatic stress.

The spatial stress field (Cauchy stress) will be obtained by pre and post multiplication of $\mathbf{F}$ as follows:

$$\boldsymbol{\sigma} = \frac{1}{J}\mathbf{F}.\mathbf{\Sigma}.\mathbf{F}^T = 2\rho_0\frac{\partial \Psi}{\partial \mathbf{g}} = \mu(\frac{1}{2}+\theta)\mathbf{b}$$

$$-\mu(\frac{1}{2}-\theta)\mathbf{b}^{-1} - \Pi_{hyd}\mathbf{g}^{-1}, \tag{11}$$

so that $\det[\mathbf{F}] = J = 1$ to satisfy the incompressibility condition.

The tangent moduli for rubber-like materials is derived as follows:

$$\mathcal{A}_{\text{hyp}} = 2\frac{\partial \mathbf{\Sigma}}{\partial \mathbf{C}} = 4\mu(\frac{1}{2}-\theta)\mathbf{I}_{C^{-1}}.\mathbf{C}^{-1} + 2\Pi_{hyd}\mathbf{I}_{C^{-1}}, \tag{12}$$

where $\mathbf{I}_{C^{-1}} = -\frac{\partial \mathbf{C}^{-1}}{\partial \mathbf{C}}$ is defined as an identity inversion of $\mathbf{C}$ and can be expanded in the following indexical form:

$$I^{ABCD}_{C^{-1}} = \frac{1}{2}(C^{-1AC}C^{-1DB} + C^{-1AD}C^{-1BC}).$$

Equilibrium Equations

The balance of linear momentum equation is the basic governing equation, here. These equations are written in material coordinates at finite strain as follows [8]:

$$\text{DIV}[(\mathbf{G}+\mathbf{H}).\mathbf{\Sigma}] = 0, \tag{13}$$

where $\mathbf{G}$, $\mathbf{H}$ and $\mathbf{\Sigma}$ are defined as before.

FIELD BOUNDARY ELEMENT METHOD

Integral Equations

The integrated form of the governing equations (Equation 13) may be represented as:

$$I = \int_\Omega \overset{*}{\mathbf{U}}.\text{DIV}[(\mathbf{H}+\mathbf{G}).\mathbf{\Sigma}]d\Omega = 0, \tag{14}$$

where Ω is the domain under consideration with boundary Γ and $\overset{*}{\mathbf{U}}$ is the fundamental Kelvin solution (see Appendix 1). Through applying the divergence theorem to the above equation, one can write the result in the form,

$$I = \int_\Gamma \overset{*}{\mathbf{U}}.(\mathbf{G}+\mathbf{H}).\mathbf{\Sigma}.\mathbf{N}d\Gamma - \int_\Omega \boldsymbol{\nabla}\overset{*}{\mathbf{U}}:[(\mathbf{G}+\mathbf{H}).\mathbf{\Sigma}]d\Omega, \tag{15}$$

so that $\boldsymbol{\nabla} = \frac{\partial}{\partial X^I}\otimes \mathbf{G}^I$ is the gradient operator. By incorporating the first part of Equation 8 in Equation 15, one would obtain:

$$\int_\Gamma \overset{*}{\mathbf{U}}.(\mathbf{G}+\mathbf{H}).\mathbf{\Sigma}.\mathbf{N}d\Gamma = \int_\Gamma \overset{*}{\mathbf{U}}.\mathbf{T}d\Gamma. \tag{16}$$

The second integral of Equation 15 is divided into two parts. Further incorporation of Equation 6 results in:

$$\int_\Omega \boldsymbol{\nabla}\overset{*}{\mathbf{U}}:[(\mathbf{G}+\mathbf{H}).\mathbf{\Sigma}]d\Omega$$

$$= \int_\Omega \boldsymbol{\nabla}\overset{*}{\mathbf{U}}:\mathbf{\Sigma}d\Omega + \int_\Omega \boldsymbol{\nabla}\overset{*}{\mathbf{U}}:(\mathbf{H}.\mathbf{\Sigma})d\Omega$$

$$= \int_\Omega \boldsymbol{\nabla}\overset{*}{\mathbf{U}}:(\mathcal{A}:\mathbf{H}+\overset{n}{\mathbf{\Sigma}})d\Omega + \int_\Omega \boldsymbol{\nabla}\overset{*}{\mathbf{U}}:(\mathbf{H}.\mathbf{\Sigma})d\Omega$$

$$= \int_\Omega \boldsymbol{\nabla}\overset{*}{\mathbf{U}}:(\mathcal{A}:\mathbf{H})d\Omega + \int_\Omega \boldsymbol{\nabla}\overset{*}{\mathbf{U}}:(\overset{n}{\mathbf{\Sigma}}+\mathbf{H}.\mathbf{\Sigma})d\Omega. \tag{17}$$

On the other hand, the fundamental stress tensor $\overset{*}{\boldsymbol{\Sigma}}$ is introduced as:

$$\overset{*}{\boldsymbol{\Sigma}} = \boldsymbol{\nabla} \overset{*}{\mathbf{U}} : \mathcal{A}. \tag{18}$$

Through substituting the constitutive relation (Equation 18) in the first integral of Equation 17, it is obtained that:

$$\int_{\Omega} \boldsymbol{\nabla} \overset{*}{\mathbf{U}} : (\mathcal{A} : \mathbf{H}) d\Omega = \int_{\Omega} \overset{*}{\boldsymbol{\Sigma}} : \mathbf{H} d\Omega = \int_{\Omega} \overset{*}{\boldsymbol{\Sigma}} : \boldsymbol{\nabla}\mathbf{U} d\Omega. \tag{19}$$

The divergence theorem, once again, may be employed, so that the integral in Equation 19 will be written as:

$$\int_{\Omega} \overset{*}{\boldsymbol{\Sigma}} : \boldsymbol{\nabla}\mathbf{U} d\Omega = \int_{\Gamma} \overset{*}{\boldsymbol{\Sigma}} . \mathbf{N} . \mathbf{U} d\Gamma - \int_{\Omega} (\mathrm{DIV}\ \overset{*}{\boldsymbol{\Sigma}}) . \mathbf{U} d\Omega. \tag{20}$$

The fundamental stress tensor is related to the fundamental traction by means of $\overset{*}{\mathbf{T}} = \overset{*}{\boldsymbol{\Sigma}} . \mathbf{N}$ which satisfies the Kelvin equation:

$$\mathrm{DIV}\ \overset{*}{\boldsymbol{\Sigma}} = - \overset{*}{\boldsymbol{\Delta}} (\mathbf{x}, \boldsymbol{\chi}),$$

where $\overset{*}{\boldsymbol{\Delta}}$ denotes the delta-Dirac function, a tensor of order 2, and $\mathbf{x}$ and $\boldsymbol{\chi}$ represent the field and source points, respectively. By imposing these identities, Equation 20 may be written as:

$$\int_{\Gamma} \overset{*}{\boldsymbol{\Sigma}} . \mathbf{N} . \mathbf{U} d\Gamma - \int_{\Omega} (\mathrm{DIV}\ \overset{*}{\boldsymbol{\Sigma}}) . \mathbf{U} = \int_{\Gamma} \overset{*}{\mathbf{T}} . \mathbf{U} d\Gamma + \mathbf{U}(\mathbf{x}). \tag{21}$$

Employing Equation 6 in the last integral of Equation 17 yields:

$$\int_{\Omega} \boldsymbol{\nabla} \overset{*}{\mathbf{U}} : (\overset{n}{\boldsymbol{\Sigma}} + \mathbf{H} . \boldsymbol{\Sigma}) d\Omega = \int_{\Omega} \boldsymbol{\nabla} \overset{*}{\mathbf{U}} : [(\mathbf{G} + \mathbf{H}) . \boldsymbol{\Sigma} - \mathcal{A} : \mathbf{H}] d\Omega. \tag{22}$$

By incorporating Equations 15 to 22 into Equation 14, the following displacement equation will be obtained:

$$\mathbf{U}(\mathbf{x}) = \int_{\Gamma} \overset{*}{\mathbf{U}} . \mathbf{T} d\Gamma - \int_{\Gamma} \overset{*}{\mathbf{T}} . \mathbf{U} d\Gamma - \int_{\Omega} \boldsymbol{\nabla} \overset{*}{\mathbf{U}} : \mathcal{N} d\Omega, \tag{23}$$

so that:

$$\mathcal{N} = (\mathbf{H} + \mathbf{G}) . \boldsymbol{\Sigma} - \mathcal{A} : \mathbf{H}. \tag{24}$$

$\mathcal{N}$ is a two-dimensional tensor which represents the summation of geometrical as well as material nonlinear terms. The displacement Equation 23 is also written for boundary nodes as:

$$\mathcal{C}(\mathbf{x}) . \mathbf{U}(\mathbf{x}) = \int_{\Gamma} \overset{*}{\mathbf{U}} . \mathbf{T} d\Gamma - \int_{\Gamma} \overset{*}{\mathbf{T}} . \mathbf{U} d\Gamma - \int_{\Omega} \boldsymbol{\nabla} \overset{*}{\mathbf{U}} : \mathcal{N} d\Omega. \tag{25}$$

$\mathcal{C}$ is a geometry tensor related to the geometry of the point on the boundary, which is obtained by a limiting procedure where the source point approaches the boundary [16-18]. Other methods for evaluating this tensor includes indirect methods such as the rigid body motion [18]. The displacement gradient is evaluated by partial differentiating of the displacement integral equation. The evaluation of the displacement gradient is a necessity due to the fact that the constitutive hyperelastic relations are written in terms of displacement gradients and hydrostatic stress Π_{hyd}. The differentiating would result in:

$$\begin{aligned} \mathbf{H}(\mathbf{x}) &= \boldsymbol{\nabla}_x \mathbf{U}(\mathbf{x}) \\ &= \int_{\Gamma} \overset{*}{\mathbf{K}} . \mathbf{T} d\Gamma - \int_{\Gamma} \overset{*}{\mathbf{D}} . \mathbf{U} d\Gamma - \int_{\Omega} \overset{*}{\mathbf{L}} : \mathcal{N} d\Omega \\ &\quad - \mathcal{F}(\mathbf{x}) : \mathcal{N}(\mathbf{x}). \end{aligned} \tag{26}$$

Deriving the kernels $\overset{*}{\mathbf{K}} = \boldsymbol{\nabla}_x \overset{*}{\mathbf{U}}$, $\overset{*}{\mathbf{L}} = \boldsymbol{\nabla}_x \boldsymbol{\nabla} \overset{*}{\mathbf{U}}$ and $\overset{*}{\mathbf{D}} = \boldsymbol{\nabla}_x \overset{*}{\mathbf{T}}$ is demonstrated in Appendix 1. $\mathcal{F}$ is called free term and is described in Appendix 2 [19].

Nonlinear Traction

In many nonlinear stress analysis, the boundary condition may vary during the deformation. When the total load is fixed in magnitude and direction, the traction changes as the boundary geometry changes. This type of nonlinear traction, which is called a follower load, has a known value in current configuration. Another nonlinear traction which is always perpendicular to the boundary and has constant distribution is called constant rotating traction.

To compute a nonlinear traction, the relations between the deformed and undeformed areas and also between the tractions in different view coordinates should be employed. For example, the relation between the Cauchy traction $\mathbf{t}$ and material traction $\mathbf{T}$ is written as:

$$\mathbf{T} = \frac{\mathrm{ds}}{\mathrm{dS}} \mathbf{Sh}^T . \mathbf{t} \ . \tag{27}$$

On the other hand, the ratio of deformed to undeformed area is [8]:

$$\frac{\mathrm{ds}}{\mathrm{dS}} = J \| [\mathbf{G} + \mathbf{H}]^{-T} . \mathbf{N} \|.$$

For the follower load conditions, one has:

$$\mathbf{T}_l = \mathbf{Sh}^T . \mathbf{t},$$

where $\mathbf{T}_l$ denotes the final traction on the deformed area ds. The difference between $\mathbf{T}$ and $\mathbf{T}_l$ provides the nonlinear traction $\mathbf{T}_\eta$, i.e.,

$$\mathbf{T}_\eta = \mathbf{T} - \mathbf{T}_l = \{ J \| [\mathbf{G} + \mathbf{H}]^{-T} . \mathbf{N} \| - 1 \} \mathbf{T}_l \ . \tag{28}$$

For the condition of constant rotating traction, the spatial traction is defined as:

$$\mathbf{t} = -p\mathbf{n},$$

where p represents the magnitude of the distribution of the spatial traction $\mathbf{t}$ along the normal direction $\mathbf{n}$. On the other hand,

$$\mathrm{nds} = J\mathbf{F}^{-T}.\mathbf{N}\mathrm{dS}. \tag{29}$$

Combining Equations 29 and 27 provides the following equation:

$$\mathbf{T} = -pJ[\mathbf{G}+\mathbf{H}]^{-T}.\mathbf{N}. \tag{30}$$

The distribution p should be unchanged in material coordinate also, thus,

$$\mathbf{T}_l = -p\mathbf{N}.$$

Consequently,

$$\mathbf{T}_\eta = \left[J(\mathbf{G}+\mathbf{H})^{-T} - \mathbf{G}\right].\mathbf{T}_l. \tag{31}$$

Incompressible Condition

An important parameter appearing in Mooney-Rivilin materials is the condition of incompressibility. This condition is mathematically represented by $\det[\mathbf{C}] = 1$, which should be satisfied for each node and must be considered as an independent equation in the overall system of equations to be solved implicitly and simultaneously. The equation is sometimes referred to as the compatibility condition which insures the uniqueness and continuity restrictions.

DISCRETIZATION

The boundary and field integrals should be evaluated numerically. In order to evaluate the coefficient matrice of displacement and tractions on the boundary, the field variables and the geometry are first described in terms of shape functions. The discretized form of Equation 25 may be obtained if ϕ and Φ are assumed to represent the boundary and field shape functions.

$$\begin{aligned} C(\mathbf{x}).U(\mathbf{x}) = &\sum_{e=1}^{ne}\sum_{i=1}^{m}\int_{\Gamma} \overset{*}{\mathbf{U}}(\mathbf{x},\boldsymbol{\chi}).[\overset{e}{\mathbf{T}}_{(i)}\ \phi_i(\beta)]\ \overset{e}{J}(\beta)d\beta \\ &- \sum_{e=1}^{ne}\sum_{i=1}^{m}\int_{\Gamma} \overset{*}{\mathbf{T}}(\mathbf{x},\boldsymbol{\chi}).[\overset{e}{\mathbf{U}}_{(i)}\ \phi_i(\beta)]\ \overset{e}{J}(\beta)d\beta \\ &- \sum_{e=1}^{Ne}\sum_{i=1}^{M}\int_{\Omega} \boldsymbol{\nabla}\overset{*}{\mathbf{U}}(\mathbf{x},\boldsymbol{\chi}) \\ &: [\overset{e}{\mathcal{N}}_{(i)}\ \Phi_i(\alpha,\beta)]\ \overset{e}{J}(\alpha,\beta)d\alpha d\beta, \end{aligned} \tag{32}$$

where ne and Ne represent the number of elements over the boundary and within domain and m and M denote the number of nodes per boundary and field element, respectively. Equation 32 may be written in the matrix form as:

$$\mathbf{K}_u\mathbf{u} = \mathbf{K}_t\mathbf{t} - \mathbf{K}_\eta\boldsymbol{\eta}, \tag{33}$$

where $\mathbf{u}$ and $\mathbf{t}$ indicate the nodal displacement and traction vectors, respectively and $\boldsymbol{\eta}$ is the nonlinear nodal vector due to nonlinear term $\mathcal{N}$. The stiffness matrices $\mathbf{K}_u$, $\mathbf{K}_t$ and $\mathbf{K}_\eta$ are obtained through numerical integration of Equation 32. $\mathbf{x}$ and $\mathbf{y}$ are considered as unknown and known variables on boundary, so that, by rearrangement of the corresponding columns of the stiffness matrices,

$$\mathbf{K}_x\mathbf{x} = \mathbf{K}_y\mathbf{y} - \mathbf{K}_\eta\boldsymbol{\eta}, \tag{34}$$

where $\mathbf{K}_x$ and $\mathbf{K}_y$ are the stiffness matrices of the known and unknown variables on the boundary.

Similar to the discretization of Equation 32, the discretized form of Equation 26 (the displacement gradient integral equation) is also obtained as:

$$\mathbf{h} = \mathbf{L}_u\mathbf{u} + \mathbf{L}_t\mathbf{t} - \mathbf{L}_\eta\boldsymbol{\eta}, \tag{35}$$

where $\mathbf{h}$ represents the nodal vector of the displacement gradient variable $\mathbf{H}$. $\mathbf{L}_u$, $\mathbf{L}_t$ and $\mathbf{L}_\eta$ are the stiffness matrices to the displacements, tractions and nonlinear terms on the boundary and the domain. A rearranging procedure is carried out to separate the known and unknown variables of the boundary vectors $\mathbf{u}$ and $\mathbf{t}$. The result is:

$$\mathbf{h} = \mathbf{L}_x\mathbf{x} + \mathbf{L}_y\mathbf{y} - \mathbf{L}_\eta\boldsymbol{\eta}. \tag{36}$$

The unknown vector $\mathbf{x}$ must be evaluated from Equation 34 and subsequently be inserted in Equation 36, so that $\mathbf{h}$ can be evaluated. $\mathbf{f}$ is defined as the residual overall vector,

$$\mathbf{f} = \mathbf{h} + \mathbf{P}_\eta\boldsymbol{\eta} - \mathbf{Q}\mathbf{y} = 0, \tag{37}$$

where the matrices $\mathbf{P}_\eta$ and $\mathbf{Q}$ are evaluated according to:

$$\begin{aligned} \mathbf{P}_\eta &= \mathbf{L}_x\mathbf{K}_x^{-1}\mathbf{K}_\eta + \mathbf{L}_\eta, \\ \mathbf{Q} &= \mathbf{L}_x\mathbf{K}_x^{-1}\mathbf{K}_y + \mathbf{L}_y. \end{aligned} \tag{38}$$

The nodal vector $\mathbf{y}$ can be divided into two different vectors, the linear part $\mathbf{y}_l$, and the nonlinear part $\mathbf{y}_\eta$. The linear part comes, for example, from the nodal kinematic (displacement) loading, and the nonlinear part may come from the nonlinear traction with its variation with respect to its direction and magnitude. Considering this definition, Equation 37 is modified as follows:

$$\mathbf{f} = \mathbf{h} + \mathbf{P}_\eta\boldsymbol{\eta} - \mathbf{Q}\mathbf{y}_\eta - \hat{\mathbf{I}}(\lambda) = 0, \tag{39}$$

where λ stands for the loading factor which can be applied incrementally. The hyperelastic analysis is not path dependent, so the loading may be exerted incrementally or totally. The relation $\hat{\mathbf{I}}(\lambda) = \mathbf{Q}\mathbf{y}_l(\lambda)$ is the solution for the linearelastic system of equations, which may be obtained as a function of the load factor. Consequently, Equation 39 may be written in terms of the unknown variable $\mathbf{h}$ and the known variables $\hat{\mathbf{I}}(\lambda)$. It should be noted that the incompressibility condition must be satisfied, together with other equations presented in Equation 39. To accomplish this, one should consider the new unknown variable Π_{hyd} to be added to the other unknown variable $\mathbf{h}$, so that the completeness of the system and uniqueness of the solution should be preserved. The overall form of the nonlinear equations is summarized as follows:

$$\mathbf{f} = \mathbf{h} + \mathbf{P}_\eta \boldsymbol{\eta}(\mathbf{h}, \pi_{hyd}) - \mathbf{Q}\mathbf{y}_\eta(\mathbf{h}, \mathbf{y}_l) - \hat{\mathbf{I}}(\mathbf{y}_l),$$

$$\mathbf{r} = \{\det \mathbf{C}(\mathbf{H}) - 1\}. \tag{40}$$

THE ITERATIVE NUMERICAL SOLUTION PROCEDURE

If the incremental loading index and the iteration index per increment are denoted by i and j, respectively, then Equation 39 can be written in indexical form as:

$$\mathbf{f}_j^i = \mathbf{h}_j^i + \mathbf{P}_\eta \boldsymbol{\eta}(\mathbf{h}, \pi_{hyd})_j^i - \mathbf{Q}\mathbf{y}_\eta(\mathbf{h}, \mathbf{y}_l)_j^i - \hat{\mathbf{I}}^i,$$

$$\mathbf{r}_j^i = \{\det \mathbf{C}(\mathbf{H}) - 1\}_j^i, \tag{41}$$

where π_{hyd} indicates the nodal vector of Π_{hyd}. For the total node number n, the total number of equations of the first and second part of Equation 41 becomes $4n$ and n, respectively.

To solve these nonlinear equations, two strategies, namely, the zero order or the fixed point iteration method and the first order tangential method are proposed. The first order tangential method has been executed through many different schemes, such as Newton-Raphson first and second order, modified Newton-Raphson and quasi-Newton methods in company with line search procedure. Although fixed point iteration methods have a reliable convergency for the nonlinear small strain or small incremental loading schemes, however, for strongly nonlinear system of equations, the rate of convergency is very poor. The first-order tangential method is more suitable for application in total-Lagrangian framework analysis. The Newton's methods require the derivatives of residual vector with respect to unknowns, which may become cumbersome in comparison with the fixed point methods.

In this paper, the basic unknowns are the nodal displacement gradients summarized in $\mathbf{h}$. The Jacobi-matrix is, therefore, given by:

$$\mathbf{J} = \frac{d\mathbf{f}}{d\mathbf{h}} = \mathbf{I} + \mathbf{P}_\eta \frac{d\boldsymbol{\eta}}{d\mathbf{h}} - \mathbf{Q}\frac{d\mathbf{y}_\eta}{d\mathbf{h}}\ . \tag{42}$$

The components of $\boldsymbol{\eta}$ are functions of the nodal variables, H_J^I and Π_{hyd} only. The matrix $\frac{\partial \boldsymbol{\eta}}{\partial \mathbf{h}}$ could be obtained in diagonal form as:

$$\begin{bmatrix} (\frac{d\mathcal{N}}{dH})_1 & 0 & \dots & 0 \\ 0 & (\frac{d\mathcal{N}}{dH})_2 & \dots & 0 \\ \dots & \dots & \dots & \dots \\ 0 & 0 & \dots & (\frac{d\mathcal{N}}{dH})_n \end{bmatrix}$$

where n is the total number of nodes and the derivatives $(\frac{d\mathcal{N}}{d\mathbf{h}})_i$ are obtained by means of the definition of $\mathcal{N}$ (given by Equation 24) as follows:

$$\begin{aligned} \frac{d\mathcal{N}^{IJ}}{dH_L^K} &= \frac{d}{dH_L^K}\{[H^I{}_M + \delta^I{}_M]\Sigma^{JM} - \mathcal{A}^{IJNP}H_{NP}\} \\ &= \delta^I{}_K\delta^L{}_M\Sigma^{JM} + [H^I{}_M + \delta^I{}_M]\frac{d\Sigma^{JM}}{dH^K{}_L} \\ &\quad - \mathcal{A}^{IJNP}\frac{d(H^Q{}_P G_{QN})}{dH^K{}_L} \\ &= \delta^I{}_K\Sigma^{JL} + [H^I{}_M + \delta^I{}_M]\frac{d\Sigma^{JM}}{dH^K{}_L} \\ &\quad - \mathcal{A}^{IJNL}G_{NK}. \end{aligned} \tag{43}$$

To evaluate the parameters in the above equation, Equation 1 and the chain rule may be used so that:

$$\frac{d\Sigma^{JM}}{dH^K{}_L} = \mathcal{A}_{\text{hyp}}{}^{JLMP}[H^N{}_P + \delta^N{}_P]G_{NK}, \tag{44}$$

where, $\mathcal{A}_{\text{hyp}}{}^{JLMP} = 2\frac{d\Sigma^{JM}}{dC_{LP}}$. Incorporating Equation 44 into Equation 43:

$$\begin{aligned} \frac{d\mathcal{N}^{IJ}}{dH^K{}_L} &= \delta^I_K\Sigma^{JL} + \{[H^I{}_M + \delta^I{}_M] \\ &\quad [H^N{}_P + \delta^N{}_P]\mathcal{A}_{hyp}{}^{MJLP} - \mathcal{A}^{IJNL}\}G_{NK}, \end{aligned} \tag{45}$$

where $\mathcal{A}_{\text{hyp}}$ is given by Equation 12. The derivative operations for matrix $\frac{d\mathbf{y}_\eta}{d\mathbf{h}}$ are complicated, for which the details are given in Appendix 3. The other derivative is $\frac{\partial \det \mathbf{C}}{\partial \mathbf{H}}$ due to incompressible condition, which is derived directly from the second equation of Equation 40 as follows:

$$\begin{aligned} \frac{\partial \det \mathbf{C}}{\partial \mathbf{H}} &= \frac{\partial \det \mathbf{C}}{\partial \mathbf{C}} : \frac{\partial \mathbf{C}}{\partial \mathbf{H}} \\ &= \det \mathbf{C}\mathbf{C}^{-1} : \frac{\partial (\mathbf{G} + \mathbf{H})^T.(\mathbf{G} + \mathbf{H})}{\partial \mathbf{H}} \\ &= 2 \det \mathbf{C}\mathbf{C}^{-1}.(\boldsymbol{\delta} + \mathbf{H}). \end{aligned} \tag{46}$$

The derivative $\frac{\partial \mathbf{f}}{\partial \boldsymbol{\pi}_{hyd}}$ can be obtained using Equation 39 together with the definition of $\mathcal{N}$ and Equation 10:

$$\frac{\partial \mathbf{f}}{\partial \boldsymbol{\pi}_{hyd}} = \mathbf{P}_{\eta} \frac{\partial \boldsymbol{\eta}}{\partial \boldsymbol{\pi}_{hyd}} = -\mathbf{P}_{\eta}\mathbf{d}, \tag{47}$$

where,

$$\mathbf{d} = \text{Diagonal}[(\mathbf{G}+\mathbf{H})^{-T}]_{n\times n}.$$

The above derivatives help in constructing the tangential matrix employed in the iterative Newton's methods. The new matrix $\boldsymbol{\Xi}$ is introduced as:

$$\boldsymbol{\Xi} = \begin{bmatrix} \frac{d\mathbf{f}}{d\mathbf{h}} & \frac{\partial \mathbf{f}}{\partial \boldsymbol{\pi}_{hyd}} \\ \frac{\partial \det \mathbf{C}}{\partial \mathbf{h}} & 0 \end{bmatrix}. \tag{48}$$

In a summarized form, the following procedure is devised to arrive at the convergent solutions of the nonlinear system of equations:

1. Let known values $\mathbf{h}$, $\boldsymbol{\pi}_{hyd}$,

   IF $\lambda_i > 1.0$ THEN EXIT.

2. Compute $\boldsymbol{\Xi}_j^{i+1}$ using Equation 48.

3. $$\begin{Bmatrix} \mathbf{h} \\ \boldsymbol{\pi}_{hyd} \end{Bmatrix}_{j+1}^{i+1} = \begin{Bmatrix} \mathbf{h} \\ \boldsymbol{\pi}_{hyd} \end{Bmatrix}_{j}^{i+1} - [\boldsymbol{\Xi}^{-1}]_j^{i+1} \begin{Bmatrix} \mathbf{f} \\ \mathbf{r} \end{Bmatrix}_j^{i+1}.$$

4. Compute the dependent variable $\boldsymbol{\Sigma}(\mathbf{H}, \Pi_{hyd})_{j+1}^{i+1}$ using Equation 10 and $\boldsymbol{\eta}(\mathbf{H}, \boldsymbol{\Sigma})_{j+1}^{i+1}$ by definition of $\mathcal{N}$, as given in Equation 24.

5. $\mathbf{f}_{j+1}^{i+1} = \mathbf{h}_{j+1}^{i+1} + \mathbf{P}_{\eta}\boldsymbol{\eta}_{j+1}^{i+1} - \hat{\mathbf{l}}^{i+1}$

   $\mathbf{r}_{j+1}^{i+1} = \{\det \mathbf{C} - 1\}_{j+1}^{i+1}$

   IF $\left\| \begin{Bmatrix} \mathbf{f} \\ \mathbf{r} \end{Bmatrix}_{j+1}^{i+1} \right\| < \epsilon$ THEN $i = i+1$ GO TO 1

   ELSE $j = j+1$ GO TO 2,

where ϵ represents the tolerance of the convergent criterion. The iteration continues until a suitable norm of the residual vector approaches a value less than a certain tolerance.

NUMERICAL EXAMPLES

To asses the algorithm and the implementation, several classical examples in hyperelastic analysis are presented in this section.

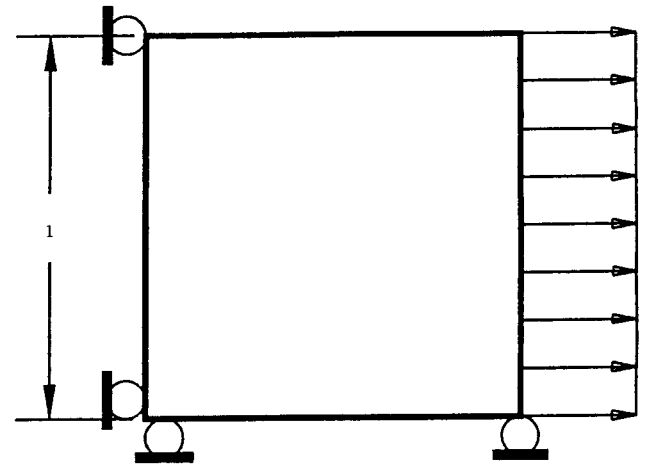

Figure 1. Initial four boundary element mesh and the dimensions.

Rubber-Like Square Plate under Tension or Compression

This example is concerned with the analysis of a simple plate made of hyperelastic rubber-like material under large deformation. A one by one square plate subjected to an incremental tensile loading is considered, as shown in Figure 1. The load is exerted by incremental displacements of up to 400% engineering strain under tension and 80% under compression. Since the loading is uniaxial in x direction, the deformation gradient can be written as follows:

$$\underbrace{\begin{bmatrix} \delta & 0 & 0 \\ 0 & 1/\delta & 0 \\ 0 & 0 & 1 \end{bmatrix}}_{\text{tension and compression}},$$

where $\delta = 1+\epsilon$ and ϵ represent the engineering strain. Under uniaxial tensile conditions, the relations between the tractions and the deformations are obtained as follows [20]:

$$t_1 = \sigma_{11} = \mu(\frac{1}{2}+\beta)\delta^2 - \mu(\frac{1}{2}-\beta)\delta^{-2} - \Pi_{hyd},$$

$$0 = \sigma_{12},$$

$$0 = \sigma_{22} = \mu(\frac{1}{2}+\beta)\delta^{-2} - \mu(\frac{1}{2}-\beta)\delta^2 - \Pi_{hyd}.$$

Eliminating Π_{hyd} from the above equations, the following traction is obtained:

$$t_1 = \mu\delta^2 - \mu\delta^{-2},$$

where t_i and σ_{ij} are, respectively, the traction and the stresses. Numerical analysis is performed by discretizing the boundary into 4 boundary elements and the domain by one bilinear element. In the execution of the problem, it is found that under such conditions, the maximum error in the Cauchy stresses

Table 1. Properties and the average number of iterations used.

Properties	$\mu = 100$ MPa			$\beta = 0.25$		
	Tension			Compression		
Number of increments	1	5	10	1	5	10
Newton-raphson	7	5.8	5.3	7	5.6	5.2
Broyden rank-1	40	12	9.5	Div	20.6	11.1

is found to be less than 2×10^{-8}. Also it has been noticed that the maximum difference in the values of nodal stresses is about 10^{-8}. This matter proves the accuracy and uniformity of the solution in very large deformation nonlinear analyses using few boundary elements. To solve the nonlinear equations, a standard Newton-Raphson and an updated Newton's method (Broyden rank-1 update) are used. The properties of material and the average iterations per increment are presented in Table 1. The very low number of iterations used shows the quadratic rate of convergency in the Newton's method. The rate of convergency decreases in compression compared with the case of tension because, under compression, instability and bifurcation may appear. Moreover, it is found that by increasing the incremental loads, the average number of iterations becomes lower. The numerical output reveals that the maximum error in Cauchy stresses is less than 2×10^{-8} when the norm of error is lowered to 10^{-14} at each increment. A 64 bits double precision should be used in computational operations to obtain such accuracy. It was also found that Broyden rank-1 update scheme performs lower convergency than Newton-Raphson scheme; however, it consumes lower execution time especially when high number of degrees of freedom is used. The relation between the components of F_{11} and the tractions t on the boundary is demonstrated in Figure 2. These data are compared with the analytical solutions given in Equation 49. The data from this equation are plotted and the accuracy is well satisfied.

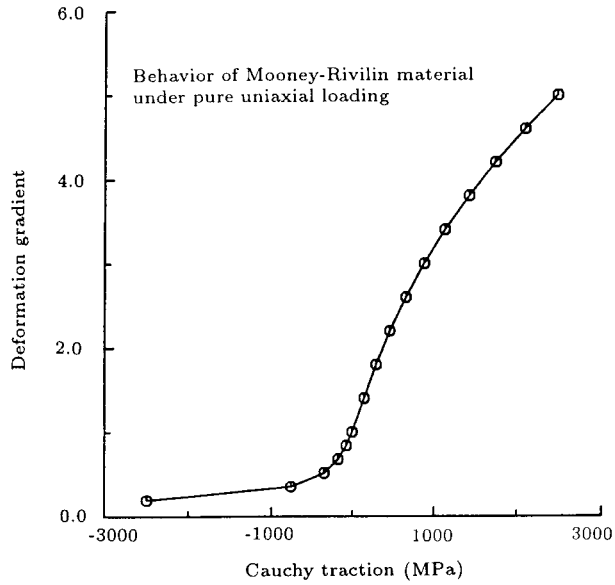

Figure 2. Relation between the deformation gradient F_{11} and the tractions t.

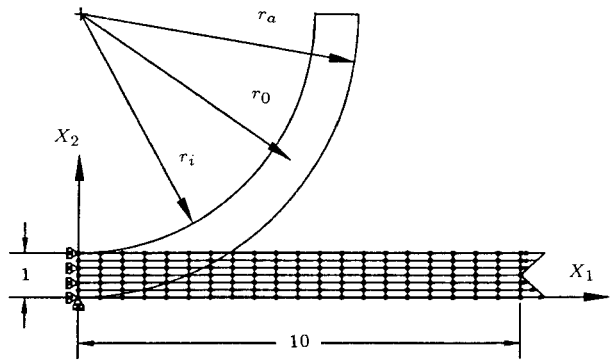

Figure 3. Initial configuration and mesh, loading, constraint and dimensions of the beam.

Bending Analysis of a Hyperelastic Beam

A hyperelastic beam under bending subjected to a pure moment at one edge and restrained at the other edge is shown in Figure 3. The properties of the beam, together with other parameters of the problem, are presented in Table 2.

By assuming Mooney-Rivilin type material for the beam and under the application of the loads and boundary conditions specified, the exact solutions are as follows [21,22]:

$$r_i = \sqrt{l\left(-\frac{h}{\theta} + \sqrt{\frac{h^2}{\theta^2} + \frac{l^2}{\theta^4}}\right)},$$

$$r_a = \sqrt{\frac{2hl}{\theta} + r_i^2} \quad \text{and} \quad \sqrt{\frac{2hlr_i r_a}{\theta(r_a^2 - r_i^2)}}. \tag{49}$$

In the above equations, r_i and r_a denote the internal and external radii of the deformed beam and r_0

Table 2. Properties, updating method, elements, nodes, increments and other parameters of Example 2.

Properties: Mooney-Rivilin	$\mu = 100$ MPa, $\beta = 0.25$
Updating scheme	Broyden rank-1
Elements on boundary and field	42 linear and 90 bilinear elements
Total nodes and degree of freedom:	112, 560
Increments, iterations and tolerance	30, 150, 10^{-12}

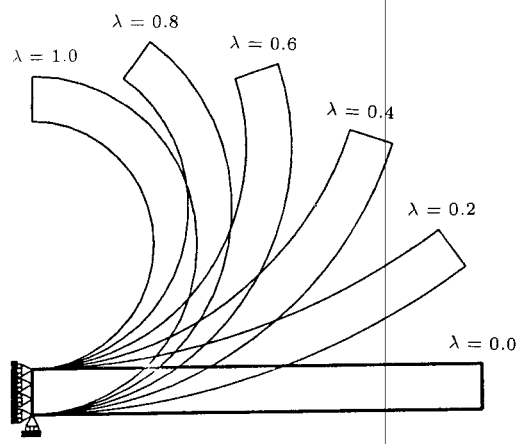

Figure 4. Exhibition of the deformed shapes of the beam in several increments of the loading.

represents the radius of stress free layer (neutral plane). Similar to the case of the plate under uniaxial loading, the finger deformation tensor appears in diagonal form as follows:

$$\mathbf{b}^{-1} = \begin{bmatrix} 1/\varsigma & 0 & 0 \\ 0 & \varsigma & 0 \\ 0 & 0 & 1 \end{bmatrix}, \quad \text{where} \quad \varsigma = \left(\frac{r\theta}{l}\right)^2. \tag{50}$$

Also, similar to the previous example, Cauchy traction is derived according to:

$$t_1 = \mu(\varsigma - \frac{1}{\varsigma}), \tag{51}$$

where t_1 is Cauchy traction in direction 1. By inserting π for θ in Equations 49 and 50 and using Equation 51, the deformed shape of the beam in the form of a semicircle, as shown in Figure 3, may be obtained. To insure the convergency and accuracy of the solution, 30 increments in the loading are chosen. Within each increment, on average, 5 iterations are used, so that the total number of iterations reaches 150. Newton's method accompanied with Broyden rank-1 update were employed to lower the error norm to less than 10^{-12}. The deformed shapes of the beam are shown in Figure 4. These deformed shapes compare very well with the predicted solutions. Moreover, the numerical outputs reveal less than 1.0% error in stress at the constraint ends compared with those of the analytically predicted solutions [20,21].

Rubber-Like Plate Containing a Circular Hole under Uniform Edge Displacements

This example deals with a four by four square plate having a circular hole at the center. The material is again assumed to be Mooney-Rivilin rubber-like. The plate is under a uniform tensile displacement (kinematical boundary conditions) applied at one edge also illustrated in Figure 5. The mesh at the initially

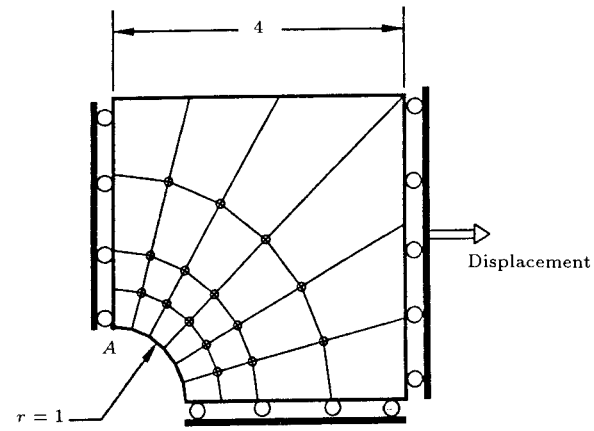

Figure 5. Initial mesh and dimension.

undeformed stage consists of 20 linear elements on the boundary and 24 bilinear elements within the domain also illustrated in Figure 5. Due to the symmetrical properties in the geometry, loading and boundary conditions, only one quarter of the body is discretized.

The loading is exerted through 20 equal incremental displacements up to 400% engineering strain, so that the total iterations reach 180 (by using Broyden rank-1 scheme). The parameters related to this example are summoned and described in Table 3. The initial undeformed and deformed shapes at several stages of loadings are shown in Figure 6. There is no exact solution for such a problem under such large deformations to compare the results with, however, they appear logical.

This example demonstrates the performance of the present algorithm for solving such nonlinear large deformation problems. The bifurcation and instability difficulties are not considered important in very large straining problems. It should be noticed that all the computational operations are carried out in reference or total Lagrangian coordinate systems.

In Figure 7, the maximum Cauchy stress at point A (point A is located on the circle boundary) is plotted against the lateral incremental displacement. From Figures 2 and 7, it can be concluded that rubber-like

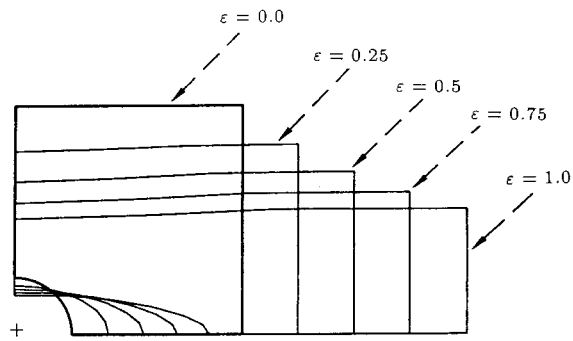

Figure 6. Initial undeformed and the deformed shapes at several stages of loading.

Table 3. Properties, elements and other features of the plate with a hole.

Types and properties of material:	Mooney-Rivilin, $\mu = 100$ MPa, $\beta = 0.25$
Nonlinear solver:	Updating Newton's method (Broyden rank-1)
Boundary elements:	20 linear boundary elements
Field elements:	24 bilinear field elements
Total nodes and degree of freedom:	35, 175
Number of increments:	20
Total number of iterations:	180
Tolerance of error norm:	10^{-13}

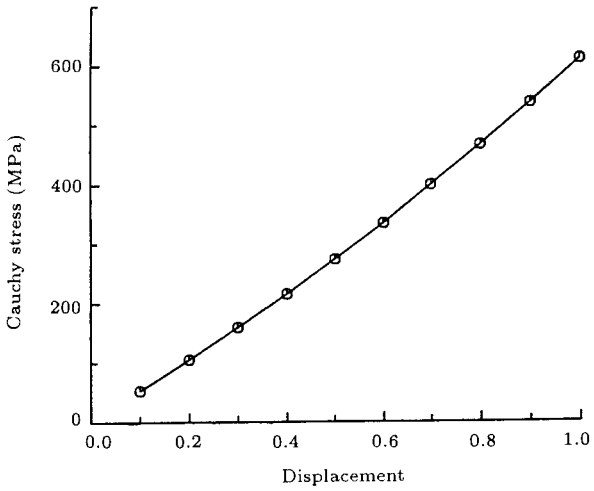

Figure 7. Relation between maximum Cauchy stress at point A and displacement.

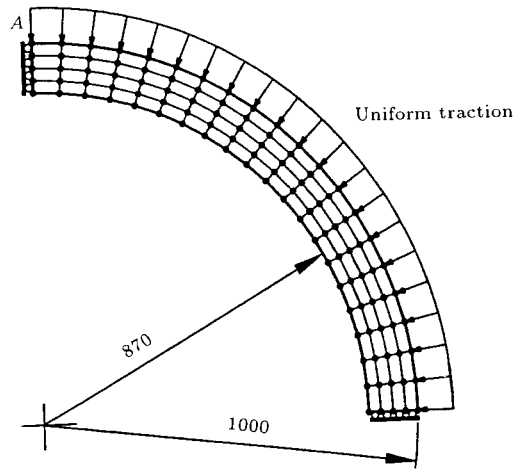

Figure 8. A quarter of a cylindrical shell with its initial mesh, dimensions and loading.

materials obey the Mooney-Rivilin behavior, having a slow progressive stiffening as long as the straining is continued. This fact means that an upward convex shape in the plot of stress vs displacement should be expected, as clearly illustrated in Figure 7.

A Cylindrical Shell under an External Hydrostatic Pressure

Figure 8 illustrates a quarter of a cylindrical shell subjected to hydrostatic pressure. The relevant dimensions and the initial mesh are also included in the figure. The material is assumed to be rubber-like, obeying Mooney-Rivilin type material behaviors. The applied pressure in this example increases until collapse, due to buckling mode, occurs suddenly. In Table 4, material, number of nodes and elements of the body and other parameters related to this example are presented.

The initial, final and several other configurations of the shell are shown in Figure 9. As shown in this figure, in the final state of the deformed shape of the shell, the first buckling mode shape is clearly observed.

The buckling happens when a significant jump in displacement of point A is observed. Point A is located at one end as shown in Figure 8. The displacement of point A vs its increasing traction is plotted in Figure 10, which clearly shows this behavior.

Table 4. Properties, elements, nodes and other parameters of the cylindrical shell.

Types and properties of material:	Mooney-Rivilin, $\mu = 100$ MPa, $\beta = 0.25$
Nonlinear solver:	Updating Newton's meth. (Broyden rank-1)
Boundary elements:	48 linear boundary elements
Field element:	80 bilinear field elements
Total nodes and degree of freedom:	105, 525
Number of increments:	Adaptive, 20 near buckling region
Total number of iterations:	30
Tolerance of error norm:	10^{-12}

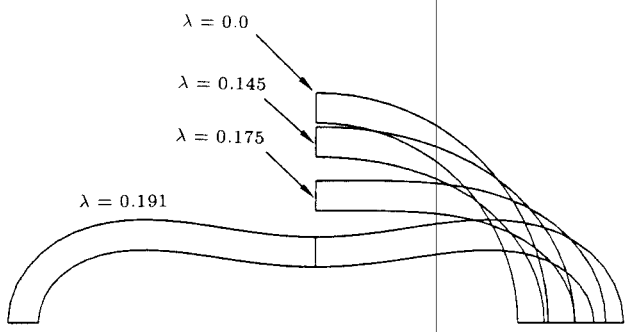

Figure 9. Initial, final and several intermediate configuration of the shell. The final configuration shows the first mode shape.

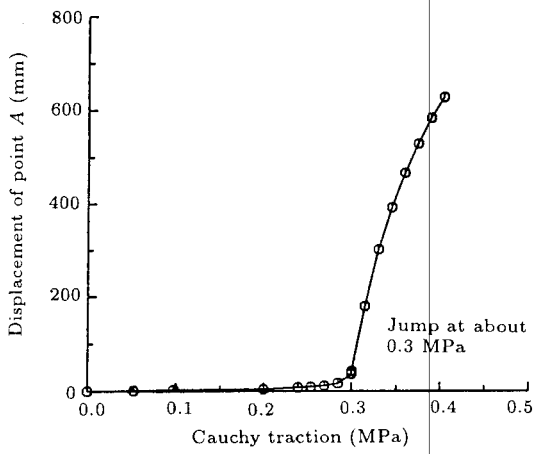

Figure 10. The displacement at point A vs its increasing traction.

Obviously an adaptive procedure should be performed by appropriately small increments to avoid missing this jump. In contrast with other buckling phenomena, sharp jumps with an asymptote may not be observed. In this case, the jump is damped when the loading is increased slowly. The value of the pressure at the jump point is 0.3 MPa, which is in close agreement with the result obtained by Foerster [22], who has reported a pressure of about 0.27 MPa at this point.

CONCLUSION

An FBEM for hyperelastic materials is presented in this paper. The formulations developed include both nonlinearities due to large deformation (geometrical) as well as the material nonlinearity. The nonlinear traction appearing on the boundary, due to change of area in magnitude and direction, are also included. Moreover, total-Lagrangian is employed which eliminates reconstruction of stiffness matrices at each incremental load step. The stiffness matrices are only evaluated at the initial configuration. Newton-Raphson and Broyden rank-1 schemes prove to have a good performance in such nonlinear numerical solutions. Several numerical examples are presented, demonstrating the efficiency of this powerful mechanized tool in the analysis of hyperelastic behavior.

REFERENCES

1. Dickey, R.W., Antman, S., *Bifurcation Problems in Nonlinear Elasticity*, Pitman publishing, New York (1971).
2. Truesdell, C., Noll, W., *The Non-Linear Field Theories of Mechanics*, in: Handbuch der Physik, Flügge, S., Springer-Verlag (1965).
3. Ogden, R.W. "Large deformation isotropic elasticity: on the correlation of theory an experiment for compressible rubber-like solids", *Proc. R. Soc. Lond. A.*, **328**, pp 567-583 (1972).
4. Ogden, R.W. "Volume changes associated with the deformation of rubber-like solids", *J. Mech. Phys. Solids*, **24**, pp 323-338 (1976).
5. Ogden, R.W. "Elastic deformations of rubber-like solids", in *Mechanics of Solids*, the Rodney Hill 60th Anniversary Volume, H.G. Hopkins and M.J. Sewell, Eds., pp 499-537 (1982).
6. Eringen, A.C., *Nonlinear Theory of Continuum Media*, McGraw-Hill, New York, USA (1962).
7. Malvern, L.E., *Introduction to the Mechanics of a Continuous Medium*, Prentice-Hall (1969).
8. Karami, G., *Principal of Linear and Nonlinear Continuum Mechanics* (to be published) (1999).
9. Simo, J.C. "A framework for finite strain elastoplasticity based on the maximum plastic dissipation and the multiplicative decomposition. Part I: continuum formulation", *Comp. Meth. Appl. Mech. Eng*, **66**, pp 199-219 (1988).
10. Simo, J.C. "A framework for finite strain elastoplasticity based on the maximum plastic dissipation and the multiplicative decomposition. Part II: computational aspects", *Comp. Meth. Appl. Mech. Eng*, **68**, pp 1-31 (1988).
11. Guiggiani, M., Krishnasamy, G., Rudolphi, T.J. and Rizzo, F.J. "A general algorithm for the numerical solution of hypersingular boundary integral equations", *Transaction of the ASME*, **59**, pp 604- 614 (1992).
12. Karami, G. and Derakhshan, D. "An efficient method to evaluate hypersingular and supersingular integrals in boundary integral equations analysis", *Eng. Anal. with Boundary Elements*, **23**, pp 317-326 (1999).
13. Guiggiani, M. and Casalini, P. "Direct computation of Cauchy principal value integral in advanced boundary element", *Int. J. Numer. Meth. Eng.*, **24**, pp 1711-1720 (1987).
14. Broyden, C.G."A class of methods for solving nonlinear simultaneous equation", *Math. Comp.*, **19**, pp 577-593 (1965).
15. Lubliner, J., *Plasticity Theory*, Macmillan, New York, USA (1990).

16. Guiggiani, M. "Hypersingular boundary integral equations have additional free term", *Computational Mechanics*, **16**, pp 245-248(1995).

17. Karami, G. "Boundary element analysis of two-dimensional elasto-plastic contact problems", *Int. J. Num. Meth. Eng.*, **36**, pp 221-236 (1993).

18. Karami, G., *A Boundary Element Method for Two-Dimensional Contact Problems*, Springer-Verlag, Berlin (1988).

19. Okada, H., Rajiyah, H. and Atluri, S.N. "Non-hypersingular integral representations for velocity (displacement) gradients in elastic-plastic solids (small or finite deformations)", *Comp. Mech.*, **4**, pp 165-175 (1989).

20. Hill, J.M. "A survey of the solved problems for rubber - Part 1 - Universal deformations", *Int. J. Mech. Eng. Ed.*, **10**(2), pp 129-140 (1982).

21. Ericksen, J.L., Rivilin, R.S. "Large elastic deformations of homogeneous anisotropic materials", *J. Rat. Mech. Anal*, **3**, pp 281-301 (1954).

22. Foerster, A. "Dissertation: Eine boundary -element-formulierung fur geometrisch und physikalisch nichtlineare probleme der feskorpermechani", Der Technischen Fakultat der Universität Erlangen-Nürnberg (1993).

APPENDIX 1

Fundamental Kernel Functions

Let $r = \sqrt{(\chi - \mathbf{x}).(\chi - \mathbf{x})}$ be the distance between source and field points. It is evident that:

$$\frac{\partial r}{\partial \mathbf{x}} = -\frac{\partial r}{\partial \chi}.$$

By using chain rule and substituting the above equation, one can conclude that:

$$\frac{\partial \mathbf{Y}}{\partial \mathbf{x}} = \frac{\partial \mathbf{Y}}{\partial r} \otimes \frac{\partial r}{\partial \mathbf{x}} = -\frac{\partial \mathbf{Y}}{\partial r} \otimes \frac{\partial r}{\partial \chi},$$

$$= -\frac{\partial \mathbf{Y}}{\partial \chi} = \nabla_x \mathbf{Y} = -\nabla \mathbf{Y},$$

where $\mathbf{Y}$ represents any regular or singular function of $\mathbf{x}$ and χ. Therefore, all the subsequent derivatives with respect to source and field point coordinates deffer from each other by a minus sign only. By employing such an operation in derivation of the fundamental kernels, one can develop the following expression for 2D problems:

$$\overset{*}{U}_{IJ} = \frac{-1}{8\pi(1-\nu)\mu}\Big\{(3-4\nu)\ln(r)G_{IJ} - r_{,I}r_{,J}\Big\},$$

$$\overset{*}{K}_{IJM} = \frac{1}{8\pi(1-\nu)\mu r}\Big\{(3-4\nu)r_{,M}G_{IJ} - r_{,J}G_{IM} - r_{,I}G_{JM} + 2r_{,I}r_{,J}r_{,M}\Big\},$$

$$\overset{*}{L}_{IJMN} = -\frac{1}{8\pi(1-\nu)\mu r^2}2\big[(3-4\nu)r_{,M}r_{,N}G_{IJ} - r_{,J}r_{,N}G_{IM} - r_{,I}r_{,N}G_{JM} - r_{,J}r_{,M}G_{IN} - r_{,I}r_{,M}G_{JN} - r_{,I}r_{,J}G_{MN} - (3-4\nu)G_{IJ}G_{MN} + G_{IM}G_{JN} + G_{IN}G_{JM} + 8r_{,I}r_{,J}r_{,M}r_{,N},$$

$$\overset{*}{T}_{IJ} = \frac{-1}{4\pi(1-\nu)r}\Big\{\big[(1-2\nu)G_{IJ} + 2r_{,I}r_{,J}\big]r_{,K}N^K - (1-2\nu)\big[r_{,A}N_B - r_{,B}N_A\big]\Big\},$$

$$\overset{*}{D}_{IJK} = \frac{-1}{4\pi(1-\nu)r^2}\Big\{2\big[(1-2\nu)r_{,K}G_{IJ} - r_{,I}G_{JK} - r_{,J}G_{IK} + 4r_{,I}r_{,J}r_{,K}\big]r_{,M}N^M - (1-2\nu)\big[N_KG_{IJ} + N_IG_{JK} - N_JG_{IK} - 2N_Ir_{,J}r_{,K} + 2N_Jr_{,I}r_{,K}\big] - 2N_Kr_{,I}r_{,J}\Big\},$$

where G_{ij} is the metric tensor of the viewing material coordinates. μ and ν are the shear modulus and Poisson's ratio, respectively.

APPENDIX 2

Integral Free Term

To derive the free term $\mathcal{F}_{ADBC}$ presented in Equation 26, it is assumed that the source point is located in the domain. The divergence theorem is applied to transfer the field integral into a boundary one. Moreover, a circular (or spherical) boundary is considered where the center corresponds to the source point. Integration on the boundary is performed and limiting procedure is employed to cancel the vicinity radius when the radius approaches zero. The result yields the following fourth order tensor:

$$\mathcal{F}_{ADBC} = \frac{1}{16(1-\nu)\mu}\big[(7-8\nu)G_{AB}G_{CD} - G_{AD}G_{BC} - G_{AC}G_{BD}\big]$$

which can be used only for 2D analyses.

APPENDIX 3

Differentiation of Nonlinear Tractions, Followed Load and Constant Rotating Tractions with Respect to Gradient of Displacement

From linear algebra, the relation

$$\frac{\partial A^{-1_{A_B}}}{\partial A^{C_D}} = -A^{-1_{A_C}}\ A^{-1_{D_B}}, \qquad \text{(A1)}$$

is used to obtain the partial differential expression:

$$\frac{\partial}{\partial H^{C_D}}(G+H)^{-1_{A_B}} =$$

$$-(G+H)^{-1_{A_E}}\ (G+H)^{-1_{F_B}}\frac{\partial}{\partial H^{C_D}}(G+H)^{E_F}$$

$$= -(G+H)^{-1_{A_E}}\ (G+H)^{-1_{F_B}}\ \delta^{E_C}\ \delta^{D_F}$$

$$= -(G+H)^{-1_{A_C}}\ (G+H)^{-1_{D_B}}, \tag{A2}$$

having the transposed form of:

$$\frac{\partial}{\partial H^{C_D}}(G+H)^{-T_{A_B}} =$$

$$-(G+H)^{-1_{E_C}}\ (G+H)^{-1_{D_F}}\ G^{AF}\ G_{BE}\ . \tag{A3}$$

Therefore, the derivative of the nonlinear part of constant rotating traction is obtained as follows:

$$\frac{\partial}{\partial H^{B_C}}\overset{(n)}{T^A} = \frac{\partial}{\partial H^{B_C}}\left[(G+H)^{-T_{A_D}} - \delta^{A_D}\right]\overset{(l)}{T^D}$$

$$= -(G+H)^{-1_{F_B}}\ (G+H)^{-1C_E}G^{EA}\ G_{DF}\ \overset{(l)}{T^D}. \tag{A4}$$

When a followed load traction is considered, some complicated steps are needed to obtain the derivative of nonlinear tractions. As the first step, the overall derivative can be considered:

$$\frac{\partial \overset{(n)}{T^A}}{\partial H^{B_C}} = \frac{\partial}{\partial H^{B_C}}\left[J||(\mathbf{G}+\mathbf{H})^{-T}.\mathbf{N}|| - 1\right]\overset{(l)}{T^A}$$

$$= \left[\frac{\partial J}{\partial H^{B_C}}||\cdots|| + \frac{J}{2||\cdots||}\frac{\partial||\cdots||^2}{\partial H^{B_C}}\right]\overset{(l)}{T^A}, \tag{A5}$$

where:

$$||\cdots||^2 = ||(\mathbf{G}+\mathbf{H})^{-T}.\mathbf{N}||^2$$

$$= N_D N_F G^{GE}(G+H)^{-1_{D_E}}(G+H)^{-1_{F_G}}.$$

For the second step, by employing relation $\frac{\partial \det(\mathbf{A})}{\partial \mathbf{A}} = \det(\mathbf{A})\mathbf{A}^{-T}$:

$$\frac{\partial J}{\partial H^{B_C}} = \frac{\partial J}{\partial F^{e_E}}\frac{\partial}{\partial H^{B_C}}\left[Sh^{e_F}(G^{F_E}+H^{F_E})\right]$$

$$= J(G+H)^{-1_{C_B}}. \tag{A6}$$

Therefore, the derivative of Euclidian norm is derived by employing Equation A2. The result is:

$$\frac{\partial||\cdots||^2}{\partial H^{B_C}} = -N_D N_F G^{GE}$$

$$\Big[(G+H)^{-1_{D_B}}(G+H)^{-1_{C_E}}(G+H)^{-1_{F_G}}$$

$$+(G+H)^{-1_{F_B}}(G+H)^{-1D_E}(G+H)^{-1_{C_G}}\Big]. \tag{A7}$$

Thus, the overall expression is obtained by substituting Equations A6 and A7 in Equation A5. Hence,

$$\frac{\partial T^{(n)A}}{\partial H^{B_C}} = \frac{JT^{(l)A}N_D N_F G^{GE}}{2||\cdots||}$$

$$\big\{2(G+H)^{-1_{C_B}}(G+H)^{-1_{D_E}}(G+H)^{-1_{F_G}}$$

$$-(G+H)^{-1_{D_B}}(G+H)^{-1_{C_E}}(G+H)^{-1_{F_G}}$$

$$-(G+H)^{-1_{F_B}}(G+H)^{-1D_E}(G+H)^{-1_{C_G}}\big\}. \tag{A8}$$

Equations A4 and A8 are used to compute Jacobian matrix **J** when the conditions of nonlinear traction are applied to the boundary.